Journal of Applied Electrochemistry **33**: 563–569, 2003.

Ohmic interelectrode voltage drop in alumina reduction cells

H. VOGT* and H.-D. KLEINSCHRODT
TFH Berlin, University of Applied Sciences, D-13353 Berlin, Germany
*(*author for correspondence, e-mail: helmutvogt@uni.de)*

Received 2 December 2002; accepted in revised form 12 March 2003

Key words: alumina reduction cells, aluminium, gas-evolving electrodes, interelectrode resistance

Abstract

The large gas bubbles underneath the anode in Hall–Héroult cells not only affect the ohmic interelectrode resistance by decreasing the cross-sectional area available for current transport. They also exhibit a strong effect on the current distribution in the bubble-free layer, substantially increasing the resistance. Available relationships applied in aluminium industry do not take this effect into account. A review on attempts to describe the interelectrode resistance is given, and an improved relationship derived from a finite element model is presented.

List of symbols

A	electrode area (m^2)
H	macrobubble height (m)
H^{**}	microbubble height (m)
I	current (A)
j	local current density (A m^{-2})
K_1	multiplier in Equation 12
K_2	multiplier in Equation 20
K_p	multiplier in Equation 5
r	radial coordinate (m)
R	resistance (V A^{-1})
R_A	radius of the electrode area pertinent to one macrobubble (m)
R_b	macrobubble mean radius (m)
U	interelectrode voltage drop (V)
Y	interelectrode distance (m)
z	vertical coordinate (m)

Greek symbols

ε	void fraction
κ	electrical conductivity of bubble-free liquid (A V^{-1} m^{-1})
κ_{LG}	electrical conductivity of gas–liquid dispersion (A V^{-1} m^{-1})
Θ^*	macrobubble coverage (-)
Θ^{**}	microbubble coverage (-)

Subscripts

0	no bubbles in interelectrode space
1	bubble-free zone
2	bubble layer
n	number of current density vectors

1. Introduction

Various attempts have been made to compose the cell voltage of industrial alumina reduction cells from the various voltage components [1–5]. All investigations show that except for the time immediately prior to the onset of the anode effect, the largest component is the voltage drop in the melt. It is usually estimated in such a

way that the resistance of the bubble layer underneath the anode is simply added to the resistance of the pure melt in the lower part of the interelectrode gap. This space is essentially free of bubbles, and one confines the problem to assume a fully vertical, undisturbed current flow. A close look shows that this procedure is inadequate.

The aim of the present paper is to summarise the most important of the available equations for the resistance of a layer with uniformly distributed bubbles and to discuss their usefulness for Hall–Héroult cells. Then the effect of the large size of gas bubbles on the resistance of the bubble layer and particularly on the bubble-free lower zone is analysed, and an improved equation is proposed.

2. Fine bubble dispersions

Hyde and Welch [6] compiled numerous equations from the literature to describe the incremental interelectrode resistance of bubbles under horizontally orientated electrodes. However, these equations are not unconditionally applicable to alumina reduction cells.

For the case of uniform bubble distribution several theoretical equations are available of which the most familiar are those due to Maxwell [7]:

$$\frac{\kappa_{LG}}{\kappa} = 1 - \frac{3\varepsilon}{2+\varepsilon} \tag{1}$$

and Bruggeman [8]:

$$\frac{\kappa_{LG}}{\kappa} = (1-\varepsilon)^{1.5} \tag{2}$$

Obviously the controlling parameter is the volume fraction of gas ε, commonly termed the 'void fraction'. These equations were compared with each other and with further equations [9–12] from which it was shown that those differences are small compared with the uncertainty of estimating realistic ε values [10, 13–15].

3. Bubble curtain

In alumina reduction cells, as well as in most other cells, the void fractions ε varies within the interelectrode space. A variation in the flow direction only was taken into account in the classical paper by Tobias [16] to estimate the current distribution of electrodes forming the walls of such channels. Alternatively, Equations 1 and 2 can approximately be applied to a bubble layer of thickness H. This is the 'bubble curtain' adjacent to the gas-evolving electrode, whereas the remaining space is essentially free of bubbles. For this case particular equations have been derived [17–19]. If ε denotes the volume fraction of gas in the bubble layer, H its thickness and Y the interelectrode distance, the incremental resistance ΔR induced by gas bubbles may be calculated from

$$\frac{\Delta R}{R_0} = \frac{H}{Y}\left(\frac{\kappa}{\kappa_{LG}} - 1\right) \tag{3}$$

with Equation 2 leading to

$$\frac{\Delta R}{R_0} = \frac{H}{Y}\left[(1-\varepsilon)^{-1.5} - 1\right] \tag{4}$$

Alternatively, a steady variation of the void fraction [20–22] was assumed. It is now clear that all these models are useful only under particular conditions, because instabilities in the two-phase flow may easily disturb the bubble layer near the electrode. The phenomenon was studied theoretically [23, 24] and experimentally [25] and estimates of the instability conditions were proposed [26, 27]. Recent flow simulations illustrate the complexity of the processes [28].

The effect of single bubbles adhering to an electrode [29] and of a closely packed planar array of spheres [30] was studied by Sides and Tobias. It was later shown [31] that their results can be simplified by replacing void fraction ε with the bubble coverage Θ, that is, the fraction of the electrode surface shadowed by adhering bubbles,

$$\frac{\Delta R}{R_0} = \frac{H}{Y} \times 0.9015\ \Theta K_p \tag{5}$$

where $K_p = 2$–3 [29]. Another simple design equation for the incremental resistance of a bubble curtain of one bubble diameter thickness is obtained from Equation 4 by replacing the void fraction with the bubble coverage [31],

$$\varepsilon = \frac{2}{3}\Theta \tag{6}$$

Dukovic and Tobias later agreed that to achieve a close approximation, the voltage increment due to attached bubbles can be calculated solely on the basis of this area loss [32]. Further studies were conducted by Wilson and Hulme [33] and by Lanzi and Savinell [34].

4. Conventional relationships for Hall–Héroult cells

Equations of these types seem to be applicable to alumina reduction cells, because here a gas–liquid layer exists underneath the anode, whereas the rest of the interelectrode space is essentially bubble-free. If the thickness of the bubble layer equals the average height H of a single bubble and Θ^* denotes the bubble coverage of these bubbles, Equation 3, may be approximated by

$$\frac{\Delta R}{R_0} = \frac{H}{Y}\left(\frac{1}{1-\Theta^*} - 1\right) \tag{7}$$

However, there are two objections to Equation 7, one being unimportant, the other one being very significant:

It is known that in addition to those large bubbles much smaller ones with a diameter of less than 0.4 mm [35, 36] exist in contact with the anode. If these microbubbles cover a fraction Θ^{**} of the anode area not covered by macrobubbles, and their average height is H^{**}, the voltage drop is more accurately described by

$$\kappa U = \frac{I}{A}\left[\frac{H^{**}}{(1-\Theta^*)(1-\Theta^{**})} + \frac{H-H^{**}}{1-\Theta^*} + Y - H\right] \tag{8}$$

In the absence of bubbles the voltage drop is

$$\kappa U_0 = \frac{I}{A} Y \tag{9}$$

giving

$$\frac{U}{U_0} = 1 - \frac{H}{Y} + \frac{1}{1-\Theta^*}\left[\frac{H}{Y} + \frac{H^{**}}{Y}\left(\frac{1}{1-\Theta^{**}} - 1\right)\right] \tag{10}$$

A numerical estimate with $H^{**} = 0.4$ mm and realistic values of Θ^{**} shows that the microbubble resistance is negligible as previously stated [5] to result in

$$\frac{U}{U_0} = 1 + \frac{H}{Y}\left(\frac{1}{1-\Theta^*} - 1\right) = \frac{H}{Y}\frac{1}{1-\Theta^*} + \frac{Y-H}{Y} \tag{11}$$

in agreement with Equation 7. Various equations of this type have been applied [3, 6, 36–38].

The essential objection to Equations 7 or 11 remains. These equations, as well as Equations 1 and 2, are applicable only to fine distributions of the dispersed phase (gas bubbles) in the continuous phase (electrolyte liquid). This condition is commonly met for smooth gas release and if the bubble size is small compared with the dimensions of the interelectrode gap, that is, for vertical electrodes and horizontal electrodes facing upwards, whereas in aqueous electrolyte solutions small and nearly spherical bubbles with a diameter of about 0.05 mm are formed. In this case, the current outside the bubble layer is sufficiently uniformly distributed and normal to the electrode surface. Then the bubble-free volume below the bubbles has no effect on the incremental voltage drop.

The shape and size of the bubbles formed in alumina reduction cells are completely different. Contrary to some aqueous electrolyses, the anodes in aluminium production have neither slots nor holes to facilitate safe smooth gas release, and the anodes are also very large. Based partly on direct observations of alumina reduction cells, and partly on evaluation of physical gas–water models [39] it is generally accepted that at the underside of anodes near-spherical bubbles are formed, which cannot escape fast enough from the interelectrode gap and coalesce to form very large bubbles.

Moreover, the wettability of anodes in Hall–Héroult cells is poor; the contact angle in cryolite melts is much larger than in aqueous solutions. Both particularities result in extraordinarily large gas bubbles. The macrobubbles assume the form of a large sheet with a thick bubble front and a thinner long trailing portion, the height of which approaches a limiting value of about 5 mm, as is known from visual observation [38, 39] and confirmed by estimates based on property data, particularly on wettability [40]. The size of macrobubbles may grow up to 100 mm [35] or 300 mm in the longitudinal dimension of bubbles in the direction of their motion [39]. So the bubble layer moving in contact with the anode surface comprises macrobubbles, the volumes of which are given as about 130 ml [39] or up to 400 to 700 ml [41] in addition to the above mentioned microbubbles.

This geometry causes a strongly nonuniform current distribution in the bubble-free zone. The flow of the electrical current is significantly diverted from the vertical direction and substantial horizontal components exist, which contribute to an increase in the ohmic voltage drop in the bubble-free zone. A correction, unnecessary in the case of only small bubbles, is required.

5. Improved relationship for Hall–Héroult cells

Zoric and Solheim studied the anodic current distribution affected by bubbles and made numerical calculations of the incremental voltage drop expressed by a relationship applicable to their particular conditions [42]. An additional attempt, based on a mathematical model, was made explicitly taking account of the additional voltage drop in the bubble-free zone by introducing an additional term [5],

$$\frac{U}{U_0} = 1 + \frac{H}{Y}\frac{\Theta^*}{1-\Theta^*} + 0.14\,\Theta^*\frac{R_b}{Y-H} \tag{12}$$

or

$$\frac{\Delta R}{R_0} = \frac{H}{Y}\frac{\Theta^*}{1-\Theta^*} + 0.14\,\Theta^*\frac{R_b}{Y-H} \tag{13}$$

This equation is generally applicable to gas-evolving electrodes facing downwards. However, the new term is unsatisfactory, because the following conditions must be met:

$$\frac{U}{U_0} = 1 \text{ at } \Theta^* = 0 \tag{14}$$

$$\frac{U}{U_0} \to \infty \text{ at } \Theta^* \to 1 \tag{15}$$

$$\frac{U}{U_0} = 1 \text{ at } \frac{R_A}{Y-H} = 0 \tag{16}$$

$$\frac{U}{U_0} = \frac{1}{1-\Theta^*} = 1 + \frac{\Theta^*}{1-\Theta^*} \text{ at } \frac{Y-H}{R_A} = 0 \tag{17}$$

Equation 12 does not meet the conditions of Equations 16 and 17. Therefore, an extension of Equation 11

$$\frac{U}{U_0} = \frac{H}{Y}\frac{1}{1-\Theta^*} + (1+K_1)\left(\frac{Y-H}{Y}\right) = 1 + \frac{H}{Y}\left(\frac{1}{1-\Theta^*} - 1\right) + K_1\left(1-\frac{H}{Y}\right) \tag{18}$$

for the relative voltage drop and

$$\frac{\Delta R}{R_0} = \frac{H}{Y}\frac{\Theta^*}{1-\Theta^*} + K_1\left(1-\frac{H}{Y}\right) \tag{19}$$

for the relative incremental resistance is introduced. The terms on the right-hand side of Equation 19 refer separately to the bubble layer and to the bubble-free layer, respectively, where $K_1 > 0$. A form meeting all the conditions (Equations 14–17) is

$$\frac{U}{U_0} = 1 + \frac{H}{Y}\frac{\Theta^*}{1-\Theta^*} + \left(1-\frac{H}{Y}\right)\frac{\Theta^*}{1-\Theta^*}\frac{1}{1+K_2\sqrt{\Theta^*}\frac{Y-H}{R_b}} \tag{20}$$

presenting a complex, but reasonable form of the unknown factor K_1 in Equations 18 and 19.

6. Finite element method

To obtain the unknown value of K_2 in Equation 20 the real geometry of the interelectrode space with exactly one macrobubble was substituted by a model shown in

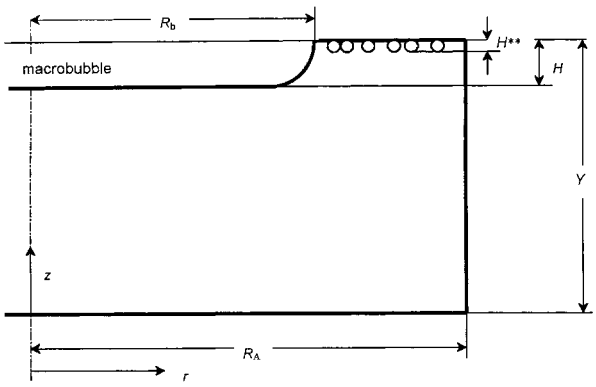

Fig. 1. Geometry of the interelectrode space.

Figure 1. The top area (anode) is partly covered by a bubble of height H and radius R_b. The radius R_A of the detail of the anode area is interrelated with the bubble radius through the macrobubble coverage

$$\Theta^* = \left(\frac{R_b}{R_A}\right)^2 \tag{21}$$

The electroactive area of the anode and the bottom area (cathode) are assumed equipotential. The field is rotationally symmetric and varies with the radius r and the height z.

The finite element method (FEM) was applied to study the form of the field and the current distribution at the cathode. Typical results are shown in Figures 2–4. It is seen from Figure 4 that the cathodic current density j in the centre of the field is small and attains a maximum value at the outer edge of the volume, $r = R_A$.

The total current results from integration of the cathodic current density values,

$$I = \int_0^{R_A} j(r)2\pi r \mathrm{d}r \tag{22}$$

approximated by a numerical integration,

$$I = \sum_{n=1}^{n_A} j_n\left(2\pi\frac{n}{n_A}R_A\right)\frac{R_A}{n_A} = 2\frac{\pi R_A^2}{n_A^2}\sum_{n=1}^{n_A} n j_n \tag{23}$$

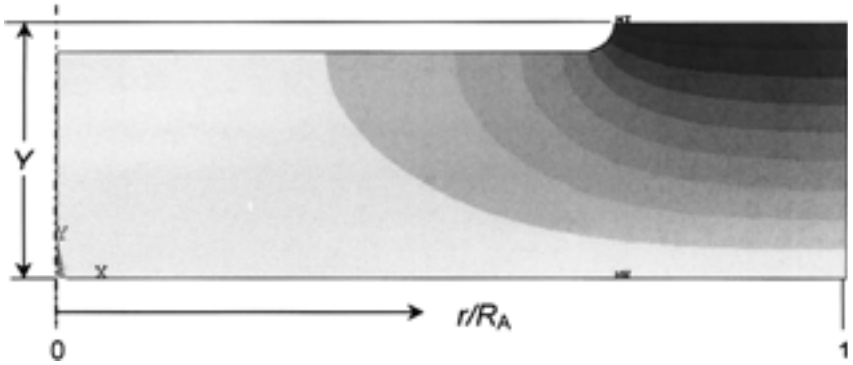

Fig. 2. Potential lines in the interelectrode space. $\Theta^* = 0.5$, $R_b = 100$ mm, $H = 5$ mm, $Y = 45$ mm.

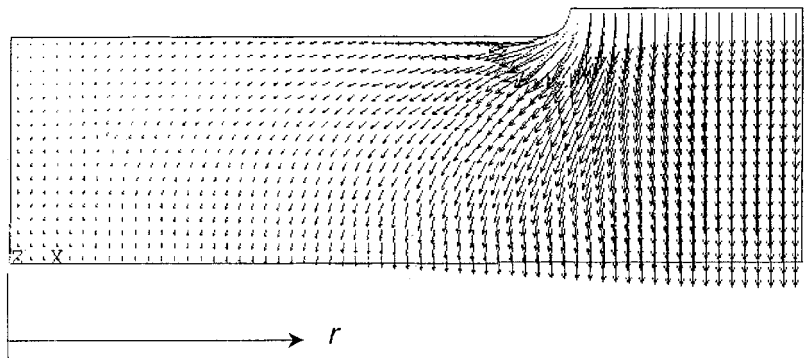

Fig. 3. Current vectors in the interelectrode space. $\Theta^* = 0.5$, $R_b = 100$ mm, $H = 5$ mm, $Y = 45$ mm.

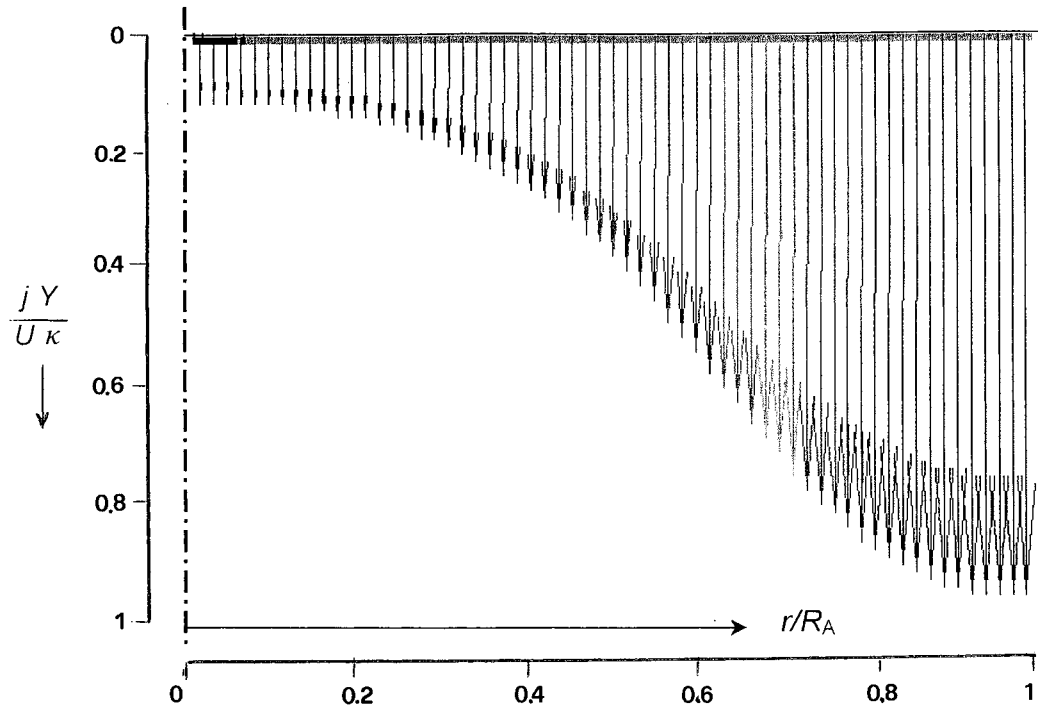

Fig. 4. Distribution of the local cathodic current density j. $\Theta^* = 0.5$, $R_b = 100$ mm, $H = 5$ mm, $Y = 45$ mm.

where n denotes the number of current density vectors from $n = 1$ near the axis to $n = n_A$ at $r = R_A$. With the voltage drop in the absence of bubbles

$$U_0 = \frac{I}{\pi R_A^2 \kappa} Y \tag{24}$$

one obtains the relative voltage drop at constant current with and without bubble as

$$\frac{I_0}{I} = \frac{U}{U_0} = \frac{U_0 \kappa}{Y} \frac{n_A^2}{2\sum_{n=1}^{n_A} n j_n} \tag{25}$$

Calculations were conducted for some selected values of the bubble coverage from the data obtained from application of FEM. Results are shown in Figure 5, illustrating the strong effect of the deviation of the current lines in the bubble-free zone. Calculated values may be approximated with high accuracy by setting $K_2 = 5$ in Equation 20 to give the ohmic voltage drop in the interelectrode space,

$$\frac{U}{U_0} = 1 + \frac{\Theta^*}{1-\Theta^*}\left(\frac{H}{Y} + \frac{1-\frac{H}{Y}}{1+5\sqrt{\Theta^*}\frac{Y-H}{R_b}}\right) \tag{26}$$

The relative incremental resistance is

$$\frac{\Delta R}{R_0} = \left(\frac{1}{1-\Theta^*} - 1\right)\left(\frac{H}{Y} + \frac{1-\frac{H}{Y}}{1+5\sqrt{\Theta^*}\frac{Y-H}{R_b}}\right) \tag{27}$$

Equations 26 and 24 are design equations for practical purposes. The major application problem is a realistic estimate of the representative bubble radius R_b and the

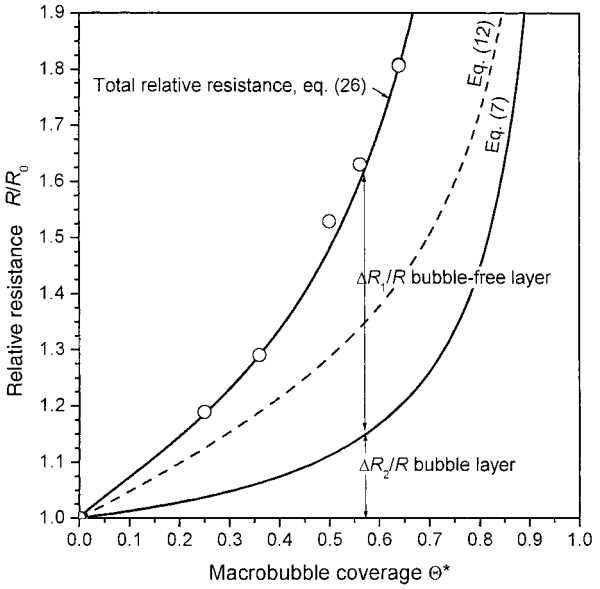

Fig. 5. Interelectrode resistance resulting from the finite element model, Equation 26, in comparison with conventional Equation 7. Broken line shows the previous attempt, Equation 12. $R_b = 100$ mm, $H = 5$ mm, $Y = 45$ mm.

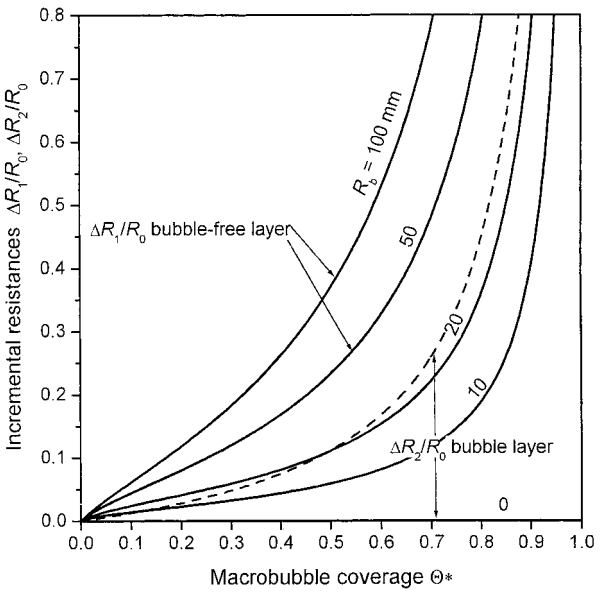

Fig. 6. Incremental resistance of the bubble-free layer (full line) and the bubble layer (dashed line). $Y = 45$ mm, $H = 5$ mm. For bubble radii $R_b > 20$ mm the incremental resistance of the bubble-free layer is larger than that of the bubble layer.

macrobubble coverage Θ*. As seen from Figure 6, the incremental resistance of the bubble-free zone is strongly affected by the macrobubble size.

Comparison with Equation 7 clearly shows that the last term in the second brackets in Equation 27 cannot be neglected, that is, the components of current flow parallel to the electrode surfaces must not be ignored. Figure 5 shows a comparison of Equations 26 or 27 with the conventional Equation 7 and the unsatisfactory attempt Equations 12 and 13.

7. Conclusion

In Hall–Héroult cells the large, flat gas bubbles in contact with anodes facing downwards substantially affect the current distribution in the bubble-free zone of the melt below the bubble layer. The common practice of neglecting the resulting increase in the incremental electrical resistance induces serious errors in the largest component of the cell voltage. The conventionally applied Equation 7 delivers values which are by far too low for industrial cells.

Equation 26 for the relative ohmic interelectrode voltage drop or Equation 27 for the incremental interelectrode resistance are recommended for practical application.

References

1. H. Ginsberg, *Chemie-Ing.-Tech.* **33** (1961) 80.
2. J. Thonstad, A. Solbu and A. Larsen, *J. Appl. Electrochem.* **1** (1971) 261.
3. W. Haupin *in* B. Welch (Ed.), 'Light Metals **1998**' (Minerals, Metals & Materials Soc., Warrendale, 1998), p. 531.
4. W. Haupin and H. Kvande *in* R.D. Peterson (Ed.), 'Light Metals **2000**' (Minerals, Metals & Materials Soc., Warrendale, 2000), p. 379.
5. H. Vogt and J. Thonstad, *J. Appl. Electrochem.* **32** (2002) 241.
6. T.M. Hyde and B.J. Welch *in* R. Huglen (Ed.), 'Light Metals **1997**' (Minerals, Metals & Materials Soc., Warrendale, 1997), p. 333.
7. J.C. Maxwell, 'A Treatise on Electricity and Magnetism', 3rd edn, Vol. 1 (Clarendon Press, Oxford 1892), p. 440; 2nd edn, Vol. 1 (Clarendon Press, Oxford, 1881), p. 435.
8. D.A.G. Bruggeman, *Ann. Physik* (*Leipzig*) **24** (1934) 626.
9. R.E. de la Rue and C.W. Tobias, *J. Electrochem. Soc.* **106** (1959) 827.
10. R.E. Meredith and C.W. Tobias, *Adv. Electrochem. Electrochem. Eng.* **2** (1962) 15.
11. S. Prager, *Physica* **29** (1963) 129.
12. J.C.R. Turner, Two-phase conductivity, *Chem. Eng. Sci.* **31** (1976) 487.
13. H. Vogt, Elektrochemische Reaktoren mit Gasentwicklung, *in* 'Fortschritte der Verfahrenstechnik', Vol. 16 (VDI-Verlag, Düsseldorf, 1 978), p. 297.
14. H. Vogt, Electrochemical reactors with gas evolution, *in* Fortschritte der Verfahrenstechnik', Vol. 20 (VDI-Verlag, Düsseldorf, 1982), p. 369
15. H. Vogt, Gas evolving electrodes, *in* E. Yeager, J.O'M. Bockris, B.E. Conway and S. Sarangapani (Eds), 'Comprehensive Treatise of Electrochemistry', Vol. 6 (Plenum, New York, 1983), p. 455.
16. C.W. Tobias, *J. Electrochem. Soc.* **106** (1959) 833.
17. R.B. MacMullin *in:* J.S. Sconce (Ed.), 'Chlorine. Its Manufacture, Properties and Uses' (Reinhold, New York, 1962), p. 157.
18. F. Hine, M. Yasuda, R. Nakamura and T. Noda, *J. Electrochem. Soc.* **122** (1975) 1185.
19. H. Vogt, *Electrochim. Acta* **26** (1981) 1311; **27** (1982) 1157.
20. L.J.J. Janssen and G.J. Visser, *J. Appl. Electrochem.* **21** (1991) 386.
21. L.J.J. Janssen and G.J. Visser, *J. Appl. Electrochem.* **21** (1991) 753.
22. L.J.J. Janssen and E. Barendrecht, *Electrochim. Acta* **28** (1983) 341.
23. H. Vogt, *Physico-Chem. Hydrodyn.* **8** (1987) 373.
24. H. Vogt, *J. Appl. Electrochem.* **29** (1999) 1155
25. H. Riegel, J. Mitrovic and K. Stephan, *J. Appl. Electrochem.* **28** (1998) 10.
26. J. Eigeldinger and H. Vogt, *Electrochim. Acta* **45** (2000) 4449.

27. R.J. Balzer and H. Vogt, *J. Electrochem. Soc*., **150** (2003) .
28. M. Raja, H.-D. Kleinschrodt and H. Vogt, Two-phase flow instability in vertical interelectrode gaps – A numerical simulation with FLOTRAN, 19th CAD-FEM Users Meeting 2001, International Congress on 'FEM Technology' (Potsdam, Germany) Vol. 1, Nr. 1.6.11.
29. P.J. Sides and C.W. Tobias, *J. Electrochem. Soc*. **127** (1980) 288.
30. P.J. Sides and C.W. Tobias, *J. Electrochem. Soc*. **129** (1982) 2715.
31. H. Vogt, *J. Appl. Electrochem*. **13** (1983) 87.
32. J. Dukovic and C.W. Tobias, *J. Electrochem. Soc*. **134** (1987) 331.
33. S.D.R. Wilson and A. Hulme, *Proc. R. Soc. Lond. A* **387** (1983) 133.
34. O. Lanzi and R.F. Savinell, *J. Electrochem. Soc*. **130** (1983) 799.
35. J. Xue and H.A. Øye *in* J. Evans (Ed.), 'Light Metals **1995**' (Minerals, Metals & Materials Soc., Warrendale, 1997), p. 265.
36. R.J. Aaberg, V. Ranum, K. Williamson and B.J. Welch, *in* R. Huglen (Ed.), 'Light Metals **1997**' (Minerals, Metals & Materials Soc., Warrendale, 1997), p. 341.
37. A. Solheim and J. Thonstad, *in* R.E. Miller (Ed.), 'Light Metals **1986**' (Metallurg Soc. AIME, Warrendale, 1986), p. 397.
38. E.W. Dewing, *Can. Metallurg. Quart*. **30** (1991) 153.
39. S. Fortin, M. Gerhardt and A.J. Gesing, *in* J.P. McGreer (Ed.), 'Light Metals **1984**' (Metallurg. Soc. AIME, Warrendale, 1984), p. 721.
40. H. Vogt, *J. Appl. Electrochem*. **29** (1999) 137.
41. N.E. Richards, *in* B. Welch (Ed.), 'Light Metals **1998**' (Minerals, Metals & Materials Soc., Warrendale, 1998), p. 521.
42. J. Zoric and A. Solheim, *J. Appl. Electrochem*. **30** (2000) 787.